FI SEVIER

Contents lists available at ScienceDirect

Biosensors and Bioelectronics

journal homepage: www.elsevier.com/locate/bios



Design, fabrication, and calibration of a micromachined thermocouple for biological applications in temperature monitoring

Onnop Srivannavit^a, Rakesh Joshi^a, Weibin Zhu^a, Bin Gong^c, Irene C. Turnbull^e, Vishwendra Patel^f, Stuart C. Sealfon^a, Theodorian Borca-Tasciuc^d, Robert D. Blitzer^{g, h}, Angelo Gaitas^{a, b, *}

- ^a The Estelle and Daniel Maggin Department of Neurology, Icahn School of Medicine at Mount Sinai, New York, NY, 10029, USA
- b BioMedical Engineering & Imaging Institute, Leon and Norma Hess Center for Science and Medicine, Icahn School of Medicine at Mount Sinai, New York, NY, 10029, USA
- ^c Department of Pathology, The University of Texas Medical Branch at Galveston, Galveston, TX, 77555, USA
- d Mechanical, Aerospace & Nuclear Engineering, School of Engineering, Rensselaer Polytechnic Institute, Jonsson Engineering Center, Troy, NY, 12180, USA
- ^e Cardiovascular Research Institute, Icahn School of Medicine at Mount Sinai, New York, NY, 10029, USA
- f Nash Family Department of Neuroscience, Icahn School of Medicine at Mount Sinai, New York, NY, 10029, USA
- E Department of Pharmacological Sciences, Icahn School of Medicine at Mount Sinai, New York, NY, 10029, USA
- h Department of Psychiatry, Icahn School of Medicine at Mount Sinai, New York, NY 10029, USA

ARTICLE INFO

Keywords: Micromachined thermocouple Biological temperature Seebeck coefficient Microfabrication Intracellular thermogenesis Thermal sensing

ABSTRACT

This paper presents a microneedle thermocouple probe designed for temperature measurements in biological samples, addressing a critical need in the field of biology. Fabricated on a Silicon-On-Insulator (SOI) wafer, the probe features a doped silicon (Si)/chrome (Cr)/gold (Au) junction, providing a high Seebeck coefficient, rapid response times, and excellent temperature resolution. The microfabrication process produces a microneedle with a triangular sensing junction. Finite Element Analysis (FEA) was employed to evaluate the thermal time constant and structural integrity in tissue, supporting the probe's suitability for biological applications. Experimental validation included temperature measurements in *ex-vivo* tissue and live Xenopus laevis oocytes. Notably, intracellular thermogenesis was detected by increasing extracellular potassium concentration to depolarize the oocyte membrane, resulting in a measurable temperature rise. These findings highlight the probe's potential as a robust tool for monitoring temperature variations in biological systems.

1. Introduction

The role of temperature in biology has been a subject of debate since the early works of classical authors including Aristotle and Empedocles, who proposed that temperature differences during embryogenesis influenced organ and sex development ((Peck, 1942;Shaw, 2014). This ancient discussion foreshadows several modern studies on the influence of temperature on biological processes and disease states (Baffou et al., 2014; Baroiller et al., 2009; Baroiller and Guiguen, 2001; Chen et al., 2015; Chretien et al., 2018; Clarke, 2003; Ferguson and Joanen, 1982; Guo et al., 2012; Ki et al., 2015; Lane, 2018; Morreale et al., 1982; Nakano et al., 2017; Okabe et al. 2012, 2018; Quint et al., 2016; Rhen and Schroeder, 2010; Shen and Wang, 2014; Sonna et al., 2002; Takei et al., 2013). Temperature fluctuations are integral to processes such as metabolism, cell division, and other cellular activities (Hildebrandt et al., 2002; Jaque et al., 2014). Cancer cells generate heat (Kuruganti and

Qi, 2002) and temperature is raised in response to infections, triggering innate and adaptive immune responses (Evans et al., 2015). Brown adipose tissue is known to produce heat in response to cold conditions (Lowell and Spiegelman, 2000; Ricquier, 2006). Additionally, neuroscience research has highlighted that even slight brain temperature variations of 1 2 °C can significantly impact memory and behavioral patterns (Rajagopal et al., 2019).

Techniques involving molecular reporters have been employed to gauge temperature gradients within cells, revealing differences of approximately 1 °C 2.9 °C between cell nuclei and cytoplasm (Nakano et al., 2017; Okabe et al. 2012, 2018; Takei et al., 2013). Remarkably, temperature differentials of up to 10 °C originating from mitochondria have been reported using temperature-sensitive fluorescence probes (Baffou et al., 2014; Chretien et al., 2018; Lane, 2018). However, despite their utility, temperature-sensitive fluorescence probes have significant limitations: they are ineffective in opaque samples, are influ-

https://doi.org/10.1016/j.bios.2024.116835

Received 27 June 2024; Received in revised form 18 September 2024; Accepted 2 October 2024 0956-5663/© 20XX

^{*} Corresponding author. The Estelle and Daniel Maggin Department of Neurology, Icahn School of Medicine at Mount Sinai, New York, NY, 10029, USA. *E-mail address*: angelo.gaitas@mssm.edu (A. Gaitas).

enced by environmental factors such as pH and ionic strength, and provide low temporal resolution (Zhou et al., 2020).

In practical applications like magnetic nanoparticle (MNP)-mediated hyperthermia, MNPs are activated by an alternating magnetic field to generate localized heat within tumors, making it an effective technique for targeted cancer therapy, including in the brain and other organs (Lian et al., 2021; Rajan and Sahu, 2020). Accurate temperature monitoring is essential to prevent damage to neighboring tissues. Temperature probes are crucial for precise tissue temperature measurements, which aid in modeling heat transfer in tissues and developing accurate hyperthermia treatment protocols.

A key tool for measuring temperatures is the thermocouple, which consists of two different electrically conductive materials, typically metals, joined at two junctions: the hot junction and the cold junction (Childs, 2001). The temperature difference between these two junctions generates an electromotive force proportional to this temperature difference, a phenomenon known as the Seebeck effect. Typically, thermocouples are made from pairs of materials with positive and negative signs of the Seebeck coefficient in order to increase the measured voltage. The distinct advantage of a thermocouple lies in its sensitivity to temperature changes solely at the thermocouple junction, rendering it unaffected by temperature fluctuations in other parts of the device (Childs, 2001). Thermocouples are also characterized by ease of calibration, insensitivity to fluid viscosity and chemical processes, nontoxicity to cells and tissues, and rapid response times. Several micromachined thermocouples have been reported (Fish et al., 1995; Gianchandani et al., 1993; Gianchandani and Najafi, 1997; Jiong et al., 2017; Li et al., 2001; Majumdar et al., 1995; Shekhawat et al., 2018); however, these are not designed for use in live tissue measurements and often lack the necessary electrical insulation for operation in such environments. Recent advancements have seen the development of standard metal junction thermocouples for biological applications (Rajagopal et al. 2018, 2019; Wang et al., 2011).

In contrast to standard metal junction thermocouples, which exhibit relatively modest Seebeck coefficients (<100 $\mu V/K$ combined Seebecks), doped Si stands out for its capacity to reach significantly higher values (Assumpcao et al., 2018; Gianchandani et al., 1993; Gianchandani and Najafi, 1997; Łaszcz et al., 2021; Van Herwaarden and Sarro, 1986; Wang et al. 2018, 2020). Notably, intrinsic Si, in its undoped state, can achieve Seebeck coefficients around 1000 $\mu V/K$. The process of doping Si, wherein impurities are introduced to alter its properties, has a marked impact on its Seebeck coefficient. Light doping can result in coefficients within the range of several hundred $\mu V/K$, enhancing electrical conductivity, which is crucial for effective thermoelectric performance. However, as the doping level increases, there is a notable reduction in the Seebeck coefficient. The balance between Seebeck coefficient and electrical conductivity ensures the functionality of the thermocouple.

This paper presents the fabrication of a thermocouple probe utilizing doped Si-Cr/Au junctions on an SOI wafer. This probe offers several key advantages, particularly beneficial for biological applications. Its miniaturized design, enabled by micromachining methods and the use of doped silicon (Si) and chrome-gold (Cr/Au) junctions, allows for precise temperature measurements within the constrained and sensitive environments of tissues and large cells. The needle-like design enhances its application by enabling effective penetration into tissues, with structural integrity allowing for measurements at depths of 1 mm and beyond. The increased Seebeck coefficient, reaching up to 447 μV/K, resulting from the combined effects of the doped silicon and the Cr/Au composite stack in the probe, leads to improved temperature sensitivity. Moreover, the rapid response time facilitates real-time monitoring of dynamic biological processes. Compared to existing solutions, which may lack necessary electrical insulation, the probe is electrically insulated. We demonstrated efficacy of this probe by accurately measuring temperature changes in ex-vivo tissue samples and live Xenopus laevis oocytes.

2. Material and methods

This probe features a cantilever with a triangular-shaped tip suspended from the chip handle. The cantilever measures 40 μm in width, 10 μm in thickness, and comes in lengths of 500 μm , 1000 μm , or 1500 μm . The chip handle has dimensions of 1500 μm in width, 685 μm in thickness, and 3700 μm in length. Fig. 1 (a) displays a scanning electron microscopy (SEM) image of the fabricated micromachined probe with a 1500 μm long cantilever. The first junction is located near the cantilever's tip, featuring a triangular shape with an area of 54 μm^2 , as shown in Fig. 1 (b). The second reference junction is situated at the chip handle. Both junctions are composed of Cr/Au (40 nm/160 nm) and doped silicon. Detailed fabrication steps are illustrated and described in Supplementary Fig. S1, Supplementary material and methods.

3. Results and discussion

3.1. Probe characterization

To measure the Seebeck coefficient, a pre-calibrated 50 μ m titanium wire was used. The wire was heated using a Keithley 2400 sourcemeter (Tektronix, USA), and at each power setting, its temperature was recorded with a 75 μ m-diameter insulated thermocouple (Omega Engineering Inc, USA). Once the wire was calibrated, a 34401A multimeter

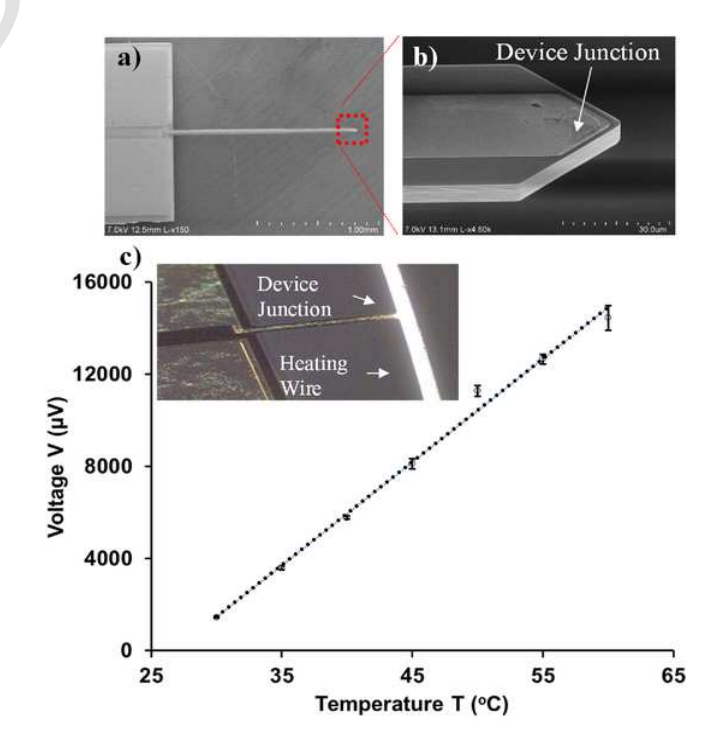


Fig. 1. Images and voltage-temperature calibration of the probe. (a) Scanning Electron Microscopy (SEM) image of the probe, which is 1500 μm in length. (b) Close-up SEM image highlighting the triangular thermocouple junction located at the tip of the cantilever probe. (c) Graph showing the relationship between the probe voltage (V) and temperature (T) obtained using a precalibrated thin wire. Each voltage measurement represents an average of 10 readings (N = 10), with the standard deviation being smaller than the size of the points on the graph and the average coefficient of variation (CV) 2.1%. The calculated Seebeck coefficient is 447 $\mu V/^{\circ} C$ (Inset) Image of the probe making contact with the calibration wire in air.

(Keysight, USA) was employed to monitor voltage changes in the probe. The probe was placed in direct contact with the wire, as shown in Supplementary Fig. S2. The wire's temperature was gradually increased and the corresponding voltage of the probe was recorded. Multiple measurements were taken for each specific power level applied to the wire.

Testing various probes using this method resulted in Seebeck coefficients ranging from 141.4 $\mu V/^{\circ}C$ to 447.3 $\mu V/^{\circ}C$ (Fig. 1(c) and Fig. S3), aligning with previous reports (Wang et al. 2018, 2020). The observed variations are likely due to differences in silicon doping, manufacturing inconsistencies, and surface effects. In comparison, commercial thermocouples, such as K-type and E-type, have lower coefficients of around 40 $\mu V/^{\circ}C$ and 68 $\mu V/^{\circ}C$, respectively. Once the Seebeck coefficient was calculated, we used this value to determine the temperature resolution of our probe. This was achieved by dividing the multimeter's resolution limit (0.1 μV) by the Seebeck coefficient (Wang et al., 2011), yielding a temperature resolution in the range of 0.0007 °C 0.00024 °C. For an analysis of the temperature fluctuations, please refer to the Supplementary Section: "Analysis of Temperature Fluctuations."

3.2. FEA simulations

The thermal time constant of the probe within tissue was determined through time-dependent numerical simulations using COMSOL Multiphysics 5.5 FEA (details described in Finite Element Modeling Supplementary Section). We employed simulations due to the limitations in the data acquisition rates of our instrumentation, a common approach in similar studies (Rajagopal et al., 2018; Wang et al., 2011) (Fig. S8). The model involved a solid tissue, where the temperature of the tissue was lower and matched that of the surrounding environment at 293 K. The dimensions of the tissue sample were specified as 2 mm by 2 mm. A convective heat flux boundary condition was applied at the interface between the tissue and the environment, assuming a heat transfer coefficient of 10 W/(m²·K) to that of air. The probe was initially set to a temperature of 313 K. Material properties for silicon (Si), gold (Au), silicon dioxide (SiO2), and tissue are detailed in Table S1. The analysis was conducted in two dimensions. Examples of the cantilever's temperature profile at time values t = 0, 10^{-5} , and 10^{-4} s are depicted in Fig. S4 (a, b, c) showing a uniform distribution of temperature across the cross section of the cantilever. Fig. 2(a) shows a magnification of the Au/Si junction area at $t = 10^{-5}$ s. The thermal time constant was estimated to be approximately $57~\mu s$, calculated from the temperature-time graph at the Au-Si junction interface (Fig. 2(b)), by identifying the point at which the temperature difference decreased to 1/e of its initial value.

To study the structural integrity of the probe we employed COMSOL Multiphysics 5.5, using its solid mechanics capabilities to conduct an analysis on a three-dimensional representation of the probe, as depicted in Fig. 2(c). The equations for linear elasticity were employed to evaluate the mechanical stresses under applied forces. The probe is a cantilever with the free end at the tip and fixed end at the base. We subjected the model to a load along the x-axis to ascertain its linear buckling threshold (Al Mamun et al., 2022; Paik et al., 2004). This analysis enabled us to calculate the critical buckling load, which is the lowest pressure that induces buckling in the probe. Our findings (Fig. S5) revealed that for a probe length of 1.5 mm, the critical buckling load was 3.46 MPa. For a probe measuring 1 mm in length, this value increased to 7.71 MPa, and for a length of 0.5 mm, the critical buckling load further increased to 30.47 MPa. These findings are particularly significant when compared against the typical resistance of human skin, which is approximately 3.18 MPa (Al Mamun et al., 2022; Fan et al., 2005; Wilke et al., 2005). This comparison suggests that all our probes possess the mechanical capability to penetrate the skin, a conclusion that is also supported by our experimental data below. This analysis focuses solely on the aspect of insertion pressure. However, for a comprehensive assessment of the probe's stability, it is essential to take into account additional factors such as bending forces and various other potential stress scenarios during insertion into the skin, which could result in mechanical failure (Aggarwal and Johnston, 2004; Al Mamun et al., 2022; Ganesan et al., 2014).

3.3. Measurement in tissues and live cells

To evaluate the performance of our probe in a biological tissue setting, we conducted temperature measurements on chicken breast tissue. A temperature controller (TEC-CH1, Nanosurf, Switzerland) was used as the heating element to apply controlled heat to the tissue. We monitored the changes in voltage from our probe using the voltmeter, as detailed in the experimental setup (Fig. S6). After inserting the thermal probe into the tissue (Fig. 3(a and b)), we gradually increased the heater's temperature to observe the tissue's internal temperature changes. For comparison, we used thermocouples: one placed at the bottom of the dish beneath the tissue and another embedded within the tissue itself (as shown in Fig. 3(b) and Fig. S6). This setup allowed us to simultaneously record temperature changes using both our probe and the reference thermocouples. Throughout the experiment, the probe remained attached to a holder and inserted into the tissue, enabling continuous temperature tracking. Additionally, the repeated insertion of the probe confirmed its durability and structural integrity. The analysis of the graph in Fig. 3(c) reveals that the temperature increases recorded

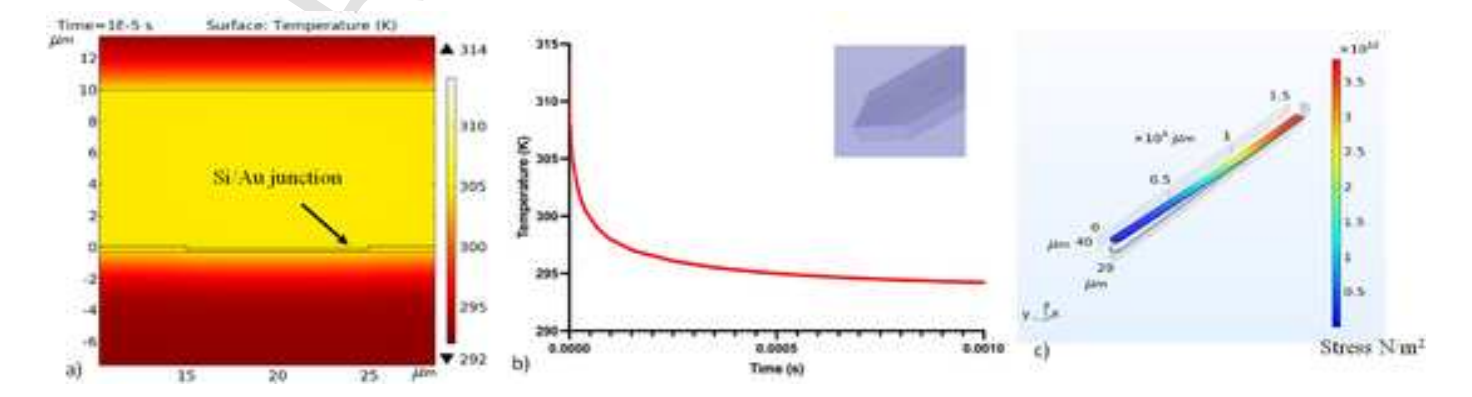


Fig. 2. FEA thermal and mechanical simulations. (a) Zoom-in view of the temperature distribution at 10^{-5} s. (b) Graph of temperature versus time at the Au-Si junction interface. (c) An FEA model utilizing the solid mechanics module was used to simulate the stress distribution. The graphical output employs color contours to depict the Von Mises stress magnitude throughout the structure. Regions experiencing elevated stress levels are highlighted in red, signifying higher intensity, whereas zones of diminished stress are conveyed through cooler (blue) tones.

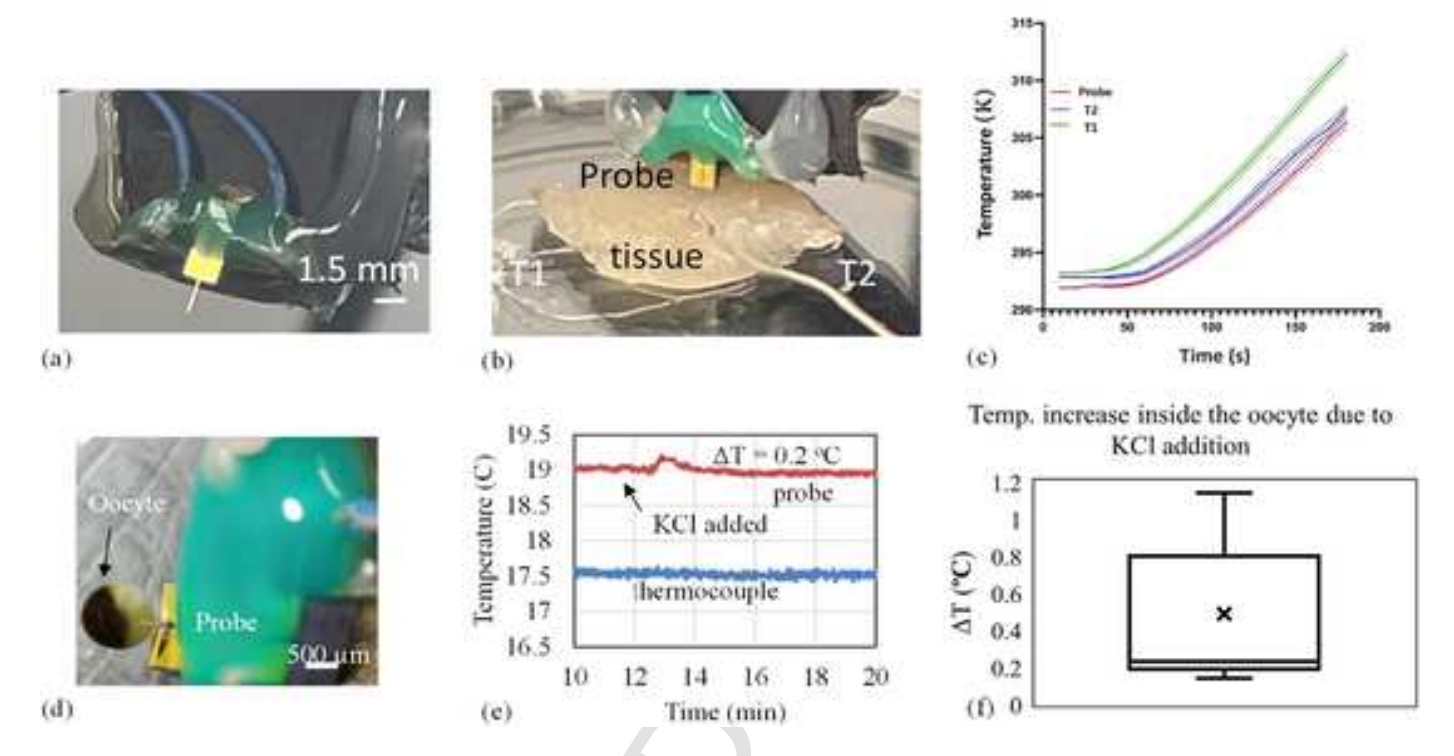


Fig. 3. Temperature measurements in biological samples. (a) Probe advancing towards the tissue. (b) Probe inserted into the tissue. (c) Temporal temperature rise of the probe and thermocouples (T1 and T2) positioned at distinct tissue sites (standard deviation shown as shaded area). Average CV for the probe is 0.097%, for T1 is 0.114%, and for T2 is 0.101%. (d) Probe positioned inside the Xenopus laevis oocyte in media. (e) Temperature response measured inside the oocyte by the probe (blue line) over a 10-min period. The red line represents the temperature recorded by a reference thermocouple placed in the surrounding media, indicating that the temperature change is localized to the oocyte. (f) Box plot summarizing the temperature change (ΔT) within the oocyte in response to KCl addition (N = 7). The central line in the box shows the median temperature increase, while the box's edges represent the interquartile range. The whiskers indicate the data's variability, and the "x" marks the mean temperature change. (CV 0.13%).

by our probe closely matched those detected by the commercial thermocouples, validating our probe's accuracy in measuring temperature within tissues. This result not only confirms the probe's effectiveness but also highlights its ability to penetrate tissue, a capability that distinguishes it from conventional thermocouples.

After testing our probe for measuring temperature changes in tissue, we moved on to assess its capability to detect small temperature changes produced by individual cells. For this purpose, we used live Xenopus laevis oocytes, which were sourced from Ecocyte Bioscience US LLC. The oocytes were kept at 4 °C in Modified Barth's Solution (MBS) supplemented with Penicillin/Streptomycin, with the solution being refreshed every 2 3 days. On the day of the experiment, a subset of oocytes was transferred to a dish. The follicle cell layer was removed using collagenase, and the fibrous vitelline envelope was carefully eliminated by incubating the oocytes in 0.05 mg/ml protease (Type VIII; Sigma) for 4 5 min (Wang, 2004). The oocytes were then allowed to equilibrate to room temperature for 2 h in 5 ml of media. Before recording oocyte temperature, nylon mesh discs (CMND-790-047, Component Supply Company, Inc., United States, 790-µm mesh opening, 54% open area, 47 mm diameter) were glued approximately 2.5 mm above the bottom surface of the dish to hold the oocytes in place. The oocytes were transferred to the dish containing the mesh. The probe was mounted on a manipulator, while a reference thermocouple was positioned on a separate manipulator to monitor the media temperature (Fig. S7). The probe was carefully inserted into the oocytes (Fig. 3 (d)). After a few minutes, we added 1 ml of potassium chloride (KCl) to achieve a final concentration of 20 µM, which induced a temperature increase. Upon KCl addition, we observed an average temperature increase of 0.49 °C with a standard deviation of 0.39 °C (N = 7) (Fig. 3(e and f)). The heating duration averaged 0.9 min with a standard deviation of 0.2 min (N = 7). To assess whether this response was physiological, a series of control experiments were performed: KCl was added to the setup without oocytes, the temperature outside the oocytes was monitored both with and without KCl, and culture media was introduced into the dish containing oocytes with the thermocouple/probe in place. No temperature changes were observed in any of the control experiments. By increasing the extracellular potassium [K+] to depolarize the oocyte membrane, various endogenous voltage-gated channels are likely activated, requiring the cells to expend additional energy to maintain homeostasis (Terhag et al., 2010). We propose that the increased metabolic demand is responsible for the observed rise in intracellular temperature.

4. Conclusions

This study introduced a novel micromachined probe on an SOI wafer for precise temperature measurements in biological tissues and cells. The probe, featuring a doped Si/Cr/Au junction, demonstrated a high Seebeck coefficient, rapid response times, and robust structural integrity, proving its suitability for biological applications. A key finding was the successful detection of intracellular thermogenesis in live Xenopus laevis oocytes, induced by high extracellular [K+] depolarization. This capability marks a significant advancement in measuring cellular temperature changes and highlights the potential of this probe for various biological research applications. While this work primarily focused on insertion pressure, future research will address other mechanical stresses to better understand the probe's stability in practical use. Limitations related to the reduced buckling load for longer probes will also

be explored by investigating material reinforcement, geometric optimization, and biocompatible coatings, aiming to enhance mechanical stability for reliable temperature measurements in deeper tissues.

CRediT authorship contribution statement

Onnop Srivannavit: Investigation, Conceptualization. Rakesh Joshi: Writing review & editing, Visualization, Validation, Investigation, Formal analysis, Data curation. Weibin Zhu: Methodology, Investigation. Bin Gong: Resources, Project administration, Investigation. Irene Turnbull: Methodology, Investigation. Vishwendra Patel: Formal analysis. Stuart C. Sealfon: Methodology, Funding acquisition. Theodorian Borca-Tasciuc: Software, Formal analysis, Data curation. Robert D. Blitzer: Formal analysis, Data curation, Conceptualization. Angelo Gaitas: Writing review & editing, Writing original draft, Visualization, Validation, Supervision, Software, Resources, Project administration, Methodology, Investigation, Funding acquisition, Formal analysis, Data curation, Conceptualization.

Declaration of competing interest

The authors declare that they have no known competing financial interests or personal relationships that could have appeared to influence the work reported in this paper.

Acknowledgements

This work was supported by the National Science Foundation under award number 226930, the National Institute of General Medical Sciences under award number R44GM146477; the content is solely the responsibility of the authors and does not necessarily represent the official views of the National Institutes of Health or the National Science Foundation. The authors extend their sincere appreciation to Prof. Takahito Ono from the Department of Mechanical Systems Engineering at Tohoku University, Sendai, Japan, for his guidance in thermocouple microfabrication and Prof. Yogesh Gianchandani from the Electrical Engineering and Computer Science Department of the University of Michigan for discussions on prior literature. The probe was fabricated at the Lurie Nanofabrication Facilities (LNF) at the University of Michigan.

Data availability

Data will be made available on request.

Appendix A. Supplementary data

Supplementary data to this article can be found online at https://doi.org/10.1016/j.bios.2024.116835.

References

Aggarwal, P., Johnston, C., 2004. Sensor. Actuator. B Chem. 102 (2), 226 234. Al Mamun, A., Sueoka, B., Allison, N., Huang, Y., Zhao, F., 2022. Sensor Actuator Phys. 336, 113407.

Assumpcao, D., Kumar, S., Narasimhan, V., Lee, J., Choo, H., 2018. Sci. Rep. 8 (1), 13725. Baffou, G., Rigneault, H., Marguet, D., Jullien, L., 2014. Nat. Methods 11 (9), 899. Baroiller, J.-F., D Cotta, H., Bezault, E., Wessels, S., Hoerstgen-Schwark, G., 2009. Comp. Biochem. Physiol. Mol. Integr. Physiol. 153 (1), 30 38.

Baroiller, J.-F., Guiguen, Y., 2001. Genes and Mechanisms in Vertebrate Sex Determination. Springer, pp. 177 201.

Chen, C., Buhl, E., Xu, M., Croset, V., Rees, J.S., Lilley, K.S., Benton, R., Hodge, J.J., Stanewsky, R., 2015. Nature 527 (7579), 516. Childs, P.R., 2001, Elsevier.

Chretien, D., Benit, P., Ha, H.-H., Keipert, S., El-Khoury, R., Chang, Y.-T., Jastroch, M., Jacobs, H.T., Rustin, P., Rak, M., 2018. PLoS Biol. 16 (1), e2003992.

Clarke, A., 2003. Trends Ecol. Evol. 18 (11), 573 581.

Evans, S.S., Repasky, E.A., Fisher, D.T., 2015. Nat. Rev. Immunol. 15 (6), 335 349.

Fan, B., Song, G., Hussain, F., 2005. Smart Mater. Struct. 14 (2), 400.

Ferguson, M.W., Joanen, T., 1982. Nature 296 (5860), 850.

Fish, G., Bouevitch, O., Kokotov, S., Lieberman, K., Palanker, D., Turovets, I., Lewis, A., 1995. Rev. Sci. Instrum. 66 (5), 3300 3306.

Ganesan, A.V., Kumar, H., Swaminathan, S., Singh, K., Joy, R.A., Sood, N., Gokhale, T., Mittal, R., 2014. Bionanoscience 4 (2), 128 135.

Gianchandani, Y., Najafi, K., Orr, B., 1993. Proceedings of IEEE International Electron Devices Meeting. IEEE, pp. 191–194.

Gianchandani, Y.B., Najafi, K., 1997. IEEE Trans. Electron. Dev. 44 (11), 1857 1868.
Guo, M., Xu, Y., Gruebele, M., 2012. Proceedings of the. National Academy of Sciences 109 (44), 17863 17867.

Hildebrandt, B., Wust, P., Ahlers, O., Dieing, A., Sreenivasa, G., Kerner, T., Felix, R., Riess, H., 2002. Crit. Rev. Oncol.-Hematol. 43 (1), 33 56.

Jaque, D., Rosal, B.d., Rodríguez, E.M., Maestro, L.M., Haro-González, P., Solé, J.G., 2014.
Nanomedicine 9 (7), 1047 1062.

Jiong, D., Jichen, W., Suijun, Y., Shuliang, Y., 2017. 2017 13th IEEE International
Conference on Electronic Measurement & Instruments (ICEMI). IEEE, pp. 168–174.
Ki, Y., Ri, H., Lee, H., Yoo, E., Choe, J., Lim, C., 2015. Neuroscientist 21 (5), 503–518.
Kuruganti, P.T., Qi, H., 2002. Proceedings of the Second Joint 24th Annual Conference

urugant, P.T., Qi, H., 2002. Proceedings of the Second Joint 24th Annual Conference and the Annual Fall Meeting of the Biomedical Engineering Society][Engineering in Medicine and Biology. IEEE, pp. 1155–1156.

Lane, N., 2018. PLoS Biol. 16 (1), e2005113.

Łaszcz, A., Czerwinski, A., Pruszyńska-Karbownik, E., Wzorek, M., Szmigiel, D., 2021. Sensors 22 (1), 287.

Li, M.-H., Wu, J.J., Gianchandani, Y.B., 2001. J. Microelectromech. Syst. 10 (1), 3 9. Lian, Y., Wang, L., Cao, J., Liu, T., Xu, Z., Yang, B., Huang, T., Jiang, X., Wu, N., 2021. Adv. Compos. Hybrid Mater. 1 13.

Lowell, B.B., Spiegelman, B.M., 2000. Nature 404 (6778), 652.

Majumdar, A., Lai, J., Chandrachood, M., Nakabeppu, O., Wu, Y., Shi, Z., 1995. Rev. Sci. Instrum. 66 (6), 3584–3592.

Morreale, S.J., Ruiz, G.J., Standora, E., 1982. Science 216 (4551), 1245 1247.

Nakano, M., Arai, Y., Kotera, I., Okabe, K., Kamei, Y., Nagai, T., 2017. PLoS One 12 (2), e0172344.

Okabe, K., Inada, N., Gota, C., Harada, Y., Funatsu, T., Uchiyama, S., 2012. Nat. Commun. 3, 705.

Okabe, K., Sakaguchi, R., Shi, B., Kiyonaka, S., 2018. Pflueg. Arch. Eur. J. Physiol. 470 (5), 717 731.

Paik, S.-J., Byun, S., Lim, J.-M., Park, Y., Lee, A., Chung, S., Chang, J., Chun, K., 2004. Sensor Actuator Phys. 114 (2 3), 276 284.

Peck, A. L., 1942. Aristotle, Generation of Animals, with an Engl. transl. Harvard University Press.

Quint, M., Delker, C., Franklin, K.A., Wigge, P.A., Halliday, K.J., van Zanten, M., 2016. Nat. Plants 2 (1), 15190.

Rajagopal, M.C., Brown, J.W., Gelda, D., Valavala, K.V., Wang, H., Llano, D.A., Gillette, R., Sinha, S., 2019. Commun. Biol. 2 (1), 1 6.

Rajagopal, M.C., Valavala, K.V., Gelda, D., Ma, J., Sinha, S., 2018. Sensor Actuator Phys. 272, 253 258.

Rajan, A., Sahu, N.K., 2020. J. Nanoparticle Res. 22, 1 $\,$ 25.

Rhen, T., Schroeder, A., 2010. Sex. Dev. 4 (1 2), 16 28.

Ricquier, D., 2006. Comptes Rendus Biol. 329 (8), 578 586.

Shaw, M.M., 2014. Research in phenomenology. 44 (2), 170 193.

Shekhawat, G.S., Ramachandran, S., Jiryaei Sharahi, H., Sarkar, S., Hujsak, K., Li, Y., Hagglund, K., Kim, S., Aden, G., Chand, A., 2018. ACS Nano 12 (2), 1760 1767.

Shen, Z.-G., Wang, H.-P., 2014. Genetics selection evolution. 46 (1), 26.

Sonna, L.A., Fujita, J., Gaffin, S.L., Lilly, C.M., 2002. J. Appl. Physiol. 92 (4), 1725 1742.
 Takei, Y., Arai, S., Murata, A., Takabayashi, M., Oyama, K., Ishiwata, S.i., Takeoka, S.,
 Suzuki, M., 2013. ACS Nano 8 (1), 198 206.

Terhag, J., Cavara, N.A., Hollmann, M., 2010. Methods 51 (1), 66 74.

Van Herwaarden, A., Sarro, P., 1986. Sensors and actuators. 10 (3 4), 321 346.

Wang, C., Xu, R., Tian, W., Jiang, X., Cui, Z., Wang, M., Sun, H., Fang, K., Gu, N., 2011. Cell Res. 21 (10), 1517.

Wang, M.H., 2004. Biochem. Biophys. Res. Commun. 324 (3), 971–972.

Wang, Z., Kimura, M., Inomata, N., Li, J., Ono, T., 2020. IEEE Sensor. J. 20 (19), 11122 11127.

Wang, Z., Kimura, M., Ono, T., 2018. Thermochim. Acta 668, 110 115.

Wilke, N., Hibert, C., O Brien, J., Morrissey, A., 2005. Sensor Actuator Phys. 123, 319, 325

Zhou, J., Del Rosal, B., Jaque, D., Uchiyama, S., Jin, D., 2020. Nat. Methods 17 (10), 967–980.